

Chenier Formation Through Wave Winnowing and Tidal Transport

Silke Tas¹, Bas van Maren², and Ad Reniers¹

¹Delft University of Technology

²Deltares

November 24, 2022

Abstract

Cheniers are ridges consisting of coarse-grained sediments, resting on top of the fine sediment that forms the otherwise muddy coast. In this paper, we use Delft3D to explore how cheniers are formed through wave winnowing. We identify three phases of chenier development: (1) a winnowing phase, during which mud is washed out of the seabed initially consisting of a mixture of sand and mud, (2) a sand transport phase, when the sand in the upper layer is transported onshore, and (3) a crest formation phase, during which a chenier crest rapidly develops at the landward limit of onshore sediment transport. The main mechanism driving onshore sand transport is wave asymmetry. During calm conditions, sand transport takes place within a narrow band limiting the volume of sand delivered nearshore, and therefore no chenier develops. In contrast, average storm conditions mobilise sufficient sand for a crest to develop. Our results thus reveal that chenier formation through wave winnowing does not require extreme storm conditions. Furthermore, our study showed that chenier formation through wave winnowing is a relatively slow process, with the largest time scales associated with the winnowing and sand transport. Once sufficient sand is available nearshore, the crest develops rapidly.

Chenier Formation Through Wave Winnowing and Tidal Transport

Silke A.J. Tas¹, D.S. van Maren^{1,2,3}, and Ad J.H.M. Reniers¹

¹Faculty of Civil Engineering and Geosciences, Delft University of Technology, Stevinweg 1, Delft 2628
CN, the Netherlands

²State Key Lab of Estuarine and Coastal Research, East China Normal University, 500 Dongchuan Rd,
Shanghai 200062, China

³Deltares, P.O. Box 177, Delft 2600 MH, the Netherlands

Key Points:

- Cheniers develop in three phases: (1) a winnowing phase, (2) an onshore sand transport phase and (3) a crest formation phase
- The main mechanism driving onshore sand transport is wave asymmetry
- Chenier formation through wave winnowing does not require extreme storm conditions

Corresponding author: Silke Tas, s.a.j.tas@tudelft.nl

Abstract

Cheniers are ridges consisting of coarse-grained sediments, resting on top of the fine sediment that forms the otherwise muddy coast. In this paper, we use Delft3D to explore how cheniers are formed through wave winnowing. We identify three phases of chenier development: (1) a winnowing phase, during which mud is washed out of the seabed initially consisting of a mixture of sand and mud, (2) a sand transport phase, when the sand in the upper layer is transported onshore, and (3) a crest formation phase, during which a chenier crest rapidly develops at the landward limit of onshore sediment transport. The main mechanism driving onshore sand transport is wave asymmetry. During calm conditions, sand transport takes place within a narrow band limiting the volume of sand delivered nearshore, and therefore no chenier develops. In contrast, average storm conditions mobilise sufficient sand for a crest to develop. Our results thus reveal that chenier formation through wave winnowing does not require extreme storm conditions. Furthermore, our study showed that chenier formation through wave winnowing is a relatively slow process, with the largest time scales associated with the winnowing and sand transport. Once sufficient sand is available nearshore, the crest develops rapidly.

Plain Language Summary

Cheniers are bodies of sand, observed along muddy coasts. Many muddy coasts worldwide suffer from erosion, but the presence of cheniers helps stabilizing the coastline and protect it against erosion. In this paper, we investigate how waves and tides create a chenier out of a mixed sand-mud bed. First, fine mud is washed out of the bed by waves, and the heavier sand grains are left behind. Then, sand is transported towards the coastline by waves. Finally, the sand accumulates in one location and a chenier is formed. Our results reveal that chenier formation does not require extreme storm conditions, but may already occur at average storm conditions. Furthermore, the first two phases (washing out the mud and transporting the sand) are relatively slow, but once sufficient sand is available nearshore, the chenier will form rapidly. The results of this study help to understand how, where and when cheniers may develop, which helps to predict the fate of (eroding) muddy coasts.

1 Introduction

Cheniers are ridges consisting of wave-reworked coarse-grained sediments, resting on top of muddy sediment (Augustinus, 1989; Otvos & Price, 1979). Cheniers may occur as a single ridge (e.g. in Demak, Indonesia) or they may be part of a chenier plain (e.g. in Louisiana, USA), where multiple clusters of cheniers, separated by mudflats, are observed. Chenier coastlines consist of mostly very fine sediments, with a small fraction of coarser grained particles, which can have a marine or fluvial origin. For example, the chenier sediment in Tourville Bay, Australia is of local, marine origin (Belperio et al., 1988) while sand in the cheniers in French Guiana originates from sand supplied by local rivers rather than from the mud banks migrating alongshore (Prost, 1989; Pujos et al., 2001; Anthony et al., 2010). Cheniers can be formed in two ways, which are related to the origin of the coarser (sandy) sediments (Augustinus, 1989). Sand can originate from winnowing, where mud is brought into suspension and the remaining sand is transported onshore through wave-driven sediment transport, accumulating in a sandy ridge. Alternatively, cheniers may develop from spits forming downdrift of river mouths. In this paper, we will focus on the first mechanism: chenier formation through wave winnowing.

Winnowing requires sufficient wave energy, for example during a storm event (Woodroffe & Grime, 1999) or during a period of increased wave action (e.g. during inter-mudbank phases along the coast of the Guianas (Anthony et al., 2010)). Furthermore, sufficient coarser-grained particles need to be available in the nearshore zone where waves create sufficiently high bed shear stresses to suspend the fines and mobilise the coarser sediments. For example, in the Louisiana Chenier Plain, cheniers are formed near the mouths of rivers discharging high fluvial sediment loads (Rosen & Xu, 2011). When higher waves coincide with spring tides, both elements (wave energy and sediment availability) are reinforced, as the waves may now rework sediments that were not available during normal conditions, e.g. the chenier formation in the Firth of Thames (Woodroffe et al., 1983; Dougherty & Dickson, 2012).

The objective of this paper is to understand how cheniers are formed through wave-induced winnowing. Despite the large amount of studies on cheniers (as in the references above) their formation is largely described in a qualitative sense, and a systematic study into chenier formation in response to wave and tidal processes is lacking. A first step towards a quantitative approach of chenier formation was made by Nardin and Fagherazzi

(2018), who studied the development of entire chenier plains using Delft3D. In this paper, we focus on the development of a single chenier, hence looking at much smaller spatial and temporal scales. We therefore deploy a process-based numerical model (Delft3D) to identify the responsible processes and mechanisms during the various phases of chenier genesis, and determine under which conditions a chenier develops. In Section 2.1 we provide an overview of the relevant sediment transport formulae and how they are implemented in Delft3D. Section 2.2 gives a brief overview of the model set-up, which is based on the model developed by Tas et al. (2022) through validation against field observations (Tas et al., 2020). We explore chenier development through a number of (idealised) scenarios described in Section 2.3. These scenarios reveal three phases of chenier formation which are presented in Section 3. The implications of our findings, as well as some limitations of our approach are discussed in Section 4 and the conclusions are presented in Section 5.

2 Methods

The formation of cheniers through wave-induced winnowing is explored using a Delft3D-FLOW morphodynamic model in combination with a SWAN wave model. Delft3D-FLOW solves the unsteady shallow water equations in two (depth-averaged) or three dimensions (Lesser et al., 2004) and SWAN is a third generation numerical wave model (Booij et al., 1999). Below (and in Appendix Appendix A) we summarize the relevant sediment transport formulae that are used to calculate sediment transport in Delft3D, followed by a description of the model set-up.

2.1 Sediment Transport in Delft3D

We consider two types of sediment: cohesive (mud) and non-cohesive (sand). Sand can be transported as bed load and as suspended load. Sediment transported as bed load is limited to a thin layer above the bed; sand particles higher in the water column are transported as suspended load. Mud is transported as suspended load or as fluid mud (for high concentrations the mud is transported as a viscous layer near the bed). Sediment transport (both sand and mud; both suspended and bed load) requires the exceedance of a critical bed shear stress to initiate movement of the sediment particles.

Bed load transport of sand is calculated using the empirical formula of van Rijn (1993). The suspended sediment transport of both mud and sand by currents are com-

108 puted with an advection-diffusion equation. Additionally, there is also suspended sand
 109 transport due to wave asymmetry, as a result of asymmetric wave orbital velocities, which
 110 is approximated following van Rijn et al. (2001). Appendix Appendix A gives an overview
 111 of the relevant sediment transport formulae.

112 2.2 Model Set-Up

113 We follow a quasi 1D approach: the model is set up in depth-averaged mode and
 114 is alongshore uniform. In order to avoid shadow effects, the WAVE-domain is much wider
 115 than the FLOW domain. The grid cell size Δx reduces from 25 m at deep water to 1.5
 116 m nearshore. The bed has a constant slope of 1:500 and consists initially of a homoge-
 117 neous mixture of 2 fractions: mostly mud and a small sand fraction ($D_{50} = 235\mu\text{m}$).
 118 The mud in Demak is very soft (with a strength of the mud layer being much too low
 119 to carry a human). Little is known about the erosion properties of such thick mud bed
 120 properties. The most similar conditions for which erosion properties of such thick fluid
 121 mud beds have been described in literature are those of van Maren, Winterwerp, and Vroom
 122 (2015), using a critical bed shear stress $\tau_{\text{cr,e}} = 0.5 \text{ N/m}^2$. Settling velocities in simi-
 123 lar environments generally range from 0.2 to 5 mm/s (Soulsby et al., 2013; Manning &
 124 Dyer, 2007; van Maren, van Kessel, et al., 2015; van Leussen & Cornelisse, 1993). Mea-
 125 surements in Demak suggested a small settling velocity on the lower end of this range
 126 (Deltares & BioManCO, 2019), hence we set $w_s = 0.5 \text{ mm/s}$. The dry bed density is
 127 typically around $\rho_{\text{dry}} = 300 \text{ kg/m}^3$. With all other parameters largely based on obser-
 128 vations or earlier work, the last remaining parameter (the erodibility parameter M_{ero})
 129 was calibrated such that the bed was dynamic but still attained dynamic equilibrium,
 130 $M_{\text{ero}} = 1.10^{-4} \text{ kg/m}^2/\text{s}$.

131 The bed composition is modelled using a layered bed stratigraphy: the bed is com-
 132 posed of multiple layers in order to account for winnowing of mud from the mixed bed.
 133 The active upper layer is 2 mm thick and always fully mixed. Upon deposition, sediments
 134 settle in the upper layer, leading to migration of sediments from the upper layer to the
 135 first bed stratigraphy layer. Only the upper layer is available for erosion, and upon ero-
 136 sion sediment from the first stratigraphy layer migrates to the active layer. The stratig-
 137 raphy layers have a maximum thickness of 10 cm, except the lowest layer when the max-
 138 imum of 10 layers is reached (this layer is limited by a non-erodible boundary 1 m be-
 139 low the initial bed level).

140 At the offshore boundary, a (time-varying) water level and wave height is prescribed
 141 (see Section 2.3 hereafter). A delayed transfer of wave energy in the landward direction
 142 is computed with a roller model (Svendsen, 1984; Nairn et al., 1991; Reniers et al., 2004).
 143 This introduces a time lag (and therefore spatial lag) between the moment of wave break-
 144 ing and the moment of energy dissipation, which is necessary for realistic modelling of
 145 cross-shore profile development of barred beaches (Reniers et al., 2004).

146 The computational time was reduced by introducing a morphological acceleration
 147 factor MorFac (multiplying the bed level change every timestep with MorFac). We have
 148 scaled the MorFac with the wave height, using a smaller factor for larger wave heights
 149 (hence larger/faster bed level changes) and verified our choice by comparing the model
 150 results with a smaller MorFac.

151 2.3 Model Scenarios

152 Boundary conditions representing the conditions in Demak, Indonesia are defined
 153 in multiple model scenarios, see Table 1. Three wave scenarios are defined: (1) sea breeze-
 154 induced waves, representing the energetic conditions during the SE monsoon season; (2)
 155 average storm conditions, which occur multiple times per NW monsoon season; and (3)
 156 extreme storm conditions, representing a storm with a return period of 10 years. The
 157 extreme storm conditions are estimated based on the peak-over-threshold analysis of Alferink
 158 (2022) performed on Wave Watch III data, which were validated against field observa-
 159 tions. A simple sinusoidal tide is prescribed at the offshore boundary, composed of the
 160 largest constituent in Demak, K1 (Tas et al., 2020), with three varying amplitudes rep-
 161 resenting no tide ($a_{K1} = 0$ m), neap tide ($a_{K1} = 0.25$ m) and spring tide ($a_{K1} = 0.5$
 162 m). The sand fraction in the initial homogeneously mixed sediment bed is varied between
 163 5, 10 and 20%. Each wave scenario is combined with any of the tidal amplitudes and sand
 164 fractions (27 scenarios). These idealised scenarios are supplemented with one scenario
 165 forced with a realistic time series for water levels and wave conditions at the offshore bound-
 166 ary (see Section 3.6).

167 3 Results

168 Figure 1 shows the formation of a chenier under constant wave conditions repre-
 169 senting average storm conditions ($H_s = 1.3$ m and $T_p = 5.6$ s, see Table 1), in the ab-
 170 sence of tide (constant water level), starting from a fully mixed bed with 10% sand. The

Table 1. Wave conditions for the three wave scenarios

Wave conditions	H_s [m]	T_p [s]	MorFac
Sea breeze	0.6	3.5	100
Average storm	1.3	5.6	25
Extreme storm	2.47	7.7	7.5

171 chenier develops in three phases: (1) winnowing, during which mud is washed out and
 172 the upper layer of the bed becomes increasingly sandy; (2) the sand in the upper layer
 173 is transported landward; and (3) crest formation, essentially the abrupt heightening of
 174 the chenier crest when sufficient sediment is available. During phase 1 and 2, when a thin
 175 sand layer is formed and transported landward, bed level changes are small; most mor-
 176 phodynamic changes take place during phase 3 when the chenier crest develops. The che-
 177 nier exemplified in Figure 1 reaches its full height after 120 days, after which the speed
 178 of bed level changes slow down.

179 Chenier development is subsequently explored for other wave conditions as well:
 180 lower waves (representing an energetic sea breeze-day during the SE monsoon season)
 181 and higher waves (representing an extreme storm). The resulting evolution of the sand
 182 fraction in the upper layer of the bed (left column, panels 2a, 2d and 2g), bed level changes
 183 (middle column, panels 2b, 2e and 2h) and sand transport (right column, panels 2c, 2f
 184 and 2i) are given in Figure 2, for extreme storm conditions (upper row), average storm
 185 conditions (middle row) and energetic sea breeze conditions (lower row) respectively.

186 For all wave scenarios, mud is winnowed from the bed and sand is subsequently trans-
 187 ported landward, but only for the higher wave scenarios a chenier crest develops (Fig-
 188 ures 2b and 2e). The sediment sorting (left column) and sand transport (right column)
 189 exhibit similar trends, which suggests that onshore sand transport depends on sand avail-
 190 ability, which is a direct result of winnowing. This landward transported sand culminates
 191 close to the shoreline and, for the higher wave conditions, develops into a chenier crest.

192 **3.1 Phase 1: Winnowing**

193 For all wave scenarios, mud is eroded over almost the entire domain (see Figure 3,
 194 left y-axis, when $|\tau_{cw,max}| - \tau_{cr,e} > 0$). However, the onset of sand transport requires

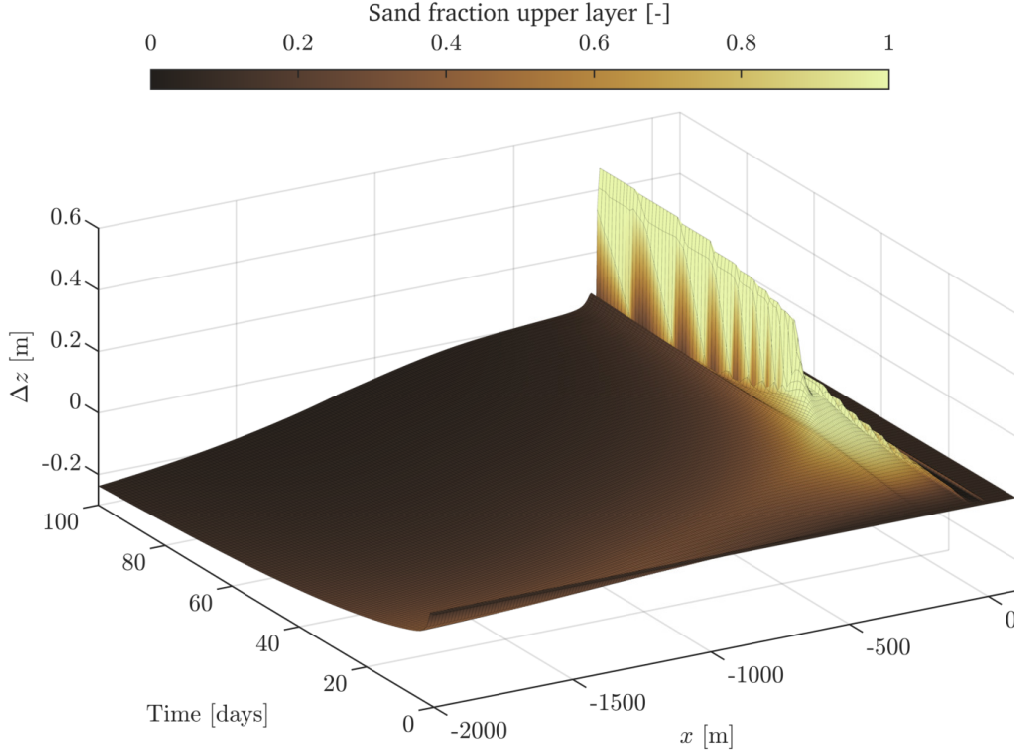


Figure 1. Changes in bed elevation and composition over time. The horizontal axes represent the time and x-coordinate (with the origin of the x-axis corresponding to the shoreline at MSL). The vertical axis represents the elevation change relative to the initial profile, and the colours represent the sand fraction of the upper layer (with 0 only mud and 1 only sand; the sand fraction of the initial mixture was equal to 0.1). The boundary conditions are constant over time, representing average storm conditions ($H_s = 1.3$ m and $T_p = 5.6$ s) and a constant water level.

195 higher flow velocities (when $|v_{\text{eff}}| - v_{\text{cr}} > 0$, right y-axis in Figure 3). This difference
 196 is especially relevant for the sea breeze scenario (Figure 3c), where mud is eroded over
 197 a much wider area, while sand is only eroded landward of $x = -900$ m. This means
 198 that seaward of $x = -900$ m, mud is being eroded from the upper bed layer, but the
 199 sand particles remain immobile, which results in a higher sand fraction in the upper bed
 200 layer (visible in Figure 2g). Landward of $x = -900$ m, both sediment fractions are mo-
 201 bilised. For higher waves (see Figures 3a-b), the erosion thresholds for both sediment frac-
 202 tions are exceeded at increasingly deeper water, resulting in erosion of both mud and sand
 203 over almost the entire domain.

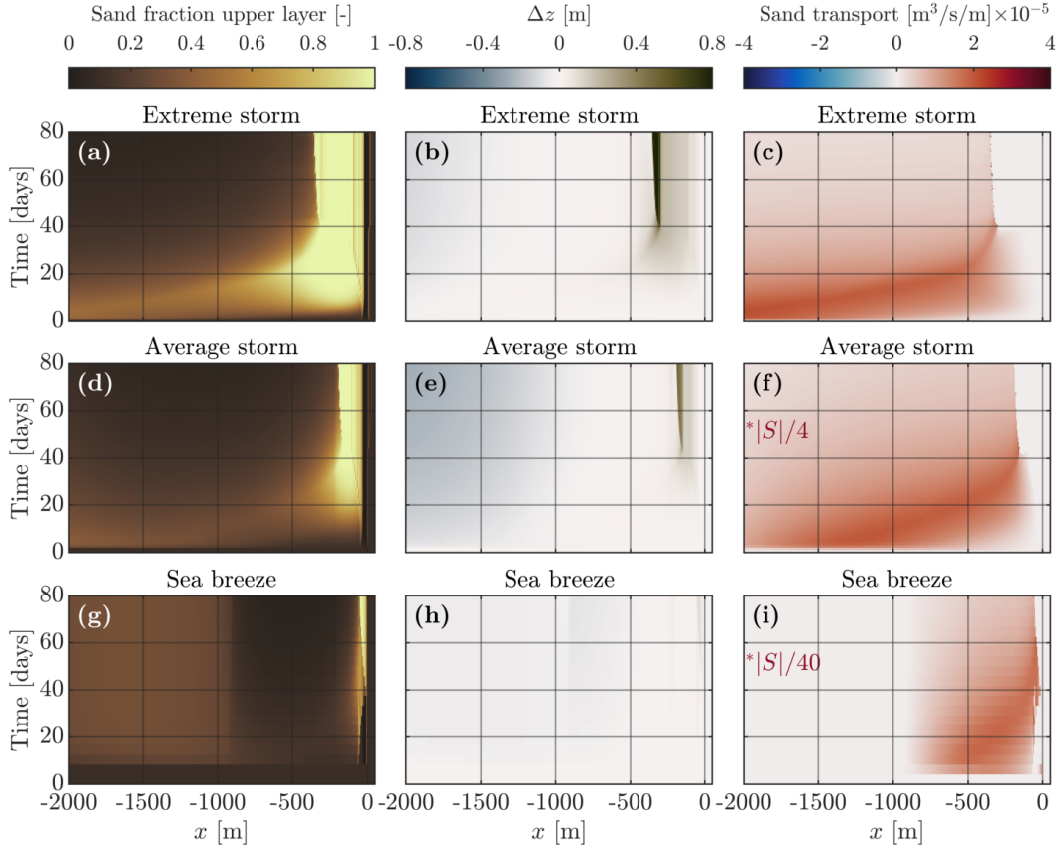


Figure 2. Evolution of the sand fraction in the upper layer (left column), the bed level change (middle column) and the sand transport (right column) for three wave scenarios (extreme storm, average storm, and sea breeze). *In order to visualize the sand transport trends for all scenarios, the colour scale is corrected with a factor 1/4 and 1/40 in panels (f) and (i), respectively (i.e. the darkest red represents a a transport of $4 \cdot 10^{-5} \text{ m}^3/\text{s}/\text{m}$ in (c), $1 \cdot 10^{-5} \text{ m}^3/\text{s}/\text{m}$ in (f) and $1 \cdot 10^{-6} \text{ m}^3/\text{s}/\text{m}$ in (i)).

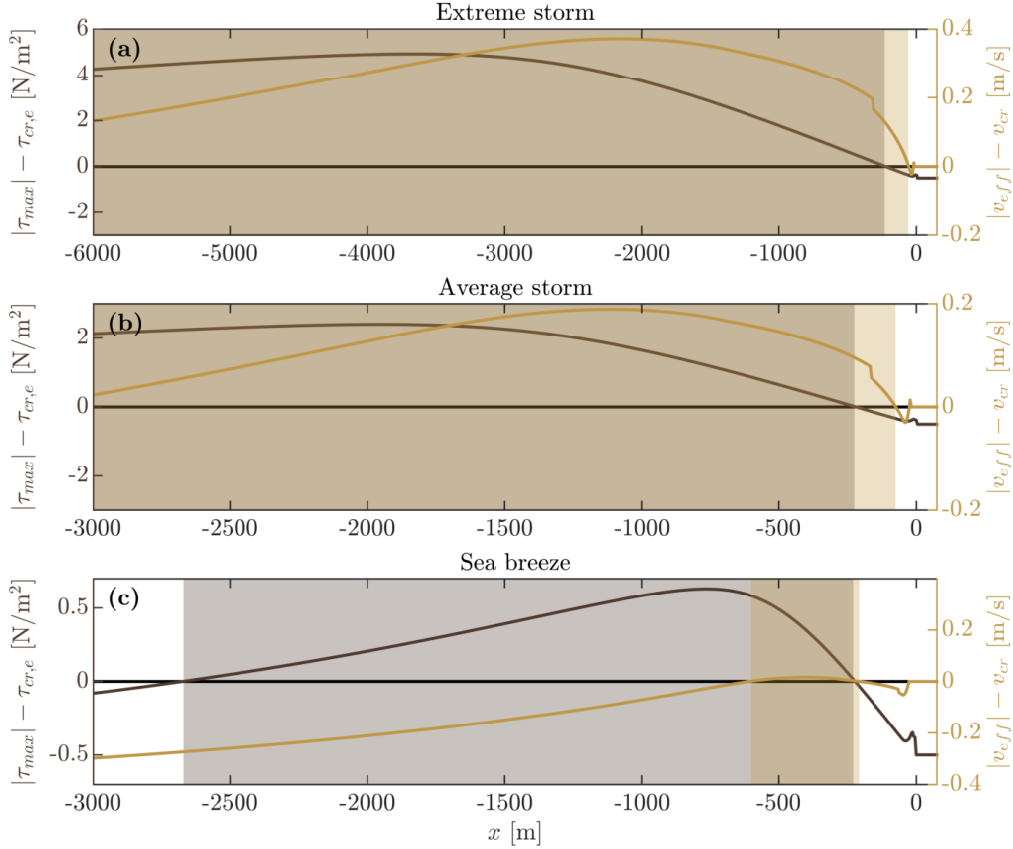


Figure 3. Visualisation of the area where the threshold for the initiation of motion is exceeded for three wave scenarios (panels a-c). Mud (dark brown, left y-axis) is eroded when $|\tau_{cw,max}| - \tau_{cr,e} > 0$ and sand (light brown, right y-axis) is eroded when $|v_{eff}| - v_{cr} > 0$.

204

3.2 Phase 2: Sand Transport

205

206

207

208

209

210

211

212

213

214

Sand transport (right column in Figure 2) is directly linked to the availability of sand in the upper layer (left column Figure 2). Sand transport is therefore supply-limited, i.e. not only governed by the transport capacity, but also by the sand availability (and thus winnowing). During phase 2, the main mechanism for onshore sand transport is wave asymmetry, as demonstrated with a simple sensitivity analysis. The modelled onshore sand transport by wave asymmetry can be modified with a user-defined parameter f_{SUSW} (calibrated to 0.5 using field observations, see Tas et al. (2022)). Applying a much lower value ($f_{SUSW} = 0.05$) results in a much lower onshore sand transport (compare panels 4a-c with panels 4d-f), revealing that onshore transport indeed results predominantly from wave asymmetry.

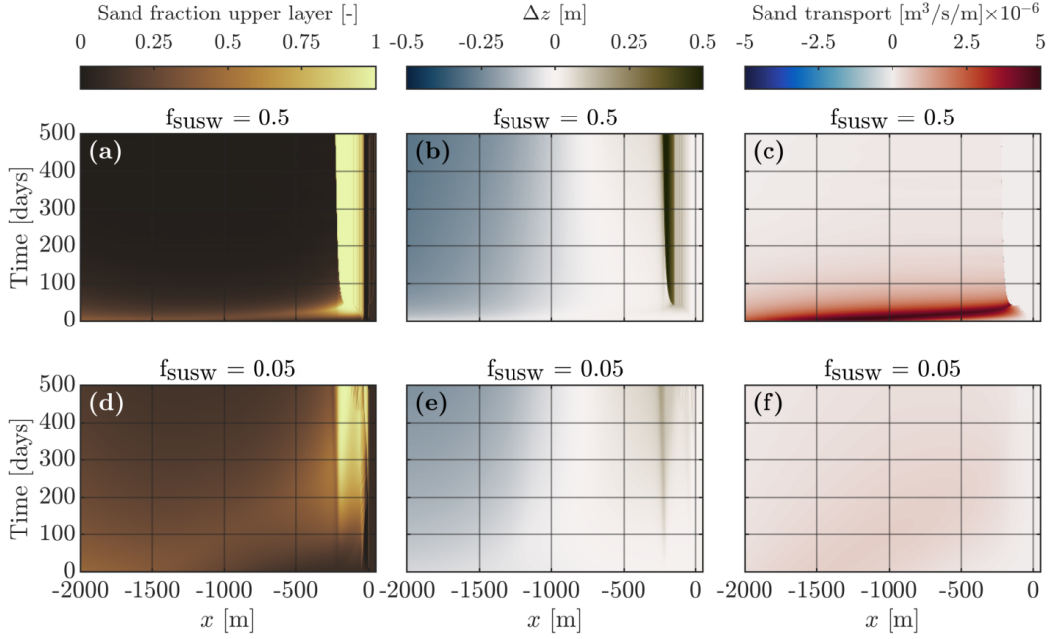


Figure 4. Sand fraction in the upper layer (left column) and total sand transport (right column) for values of $f_{\text{susw}} = 0.5$ (upper row) and $f_{\text{susw}} = 0.05$ (lower row).

215 Although there is still some onshore sand transport for the scenario with a ten times
 216 smaller value for f_{susw} (Figure 4f), leading to a sandy region near the shoreline (Fig-
 217 ure 4d), the total volume of onshore sand transport and resulting bathymetric change
 218 (Figure 4e) is small.

219 3.3 Phase 3: Crest Formation

220 The last phase of chenier formation is rapid sand accumulation at one location, thereby
 221 shaping a chenier crest. This process is very fast and abrupt: once a certain threshold
 222 is exceeded, the crest height rapidly increases.

223 Sedimentation (and erosion) can be directly linked to sediment transport gradients.
 224 A negative transport gradient is defined as a landward decrease in sediment transport,
 225 resulting in sediment deposition. Figure 5 shows the bed level change (left column), the
 226 sand transport (middle column) and the sand transport gradient (right column) for a
 227 scenario during average storm conditions. The three rows show a different initial sand
 228 content, in this section we focus on the middle row (sand content of 10%), the other rows
 229 (5% and 20% sand) will be discussed in Section 3.4.

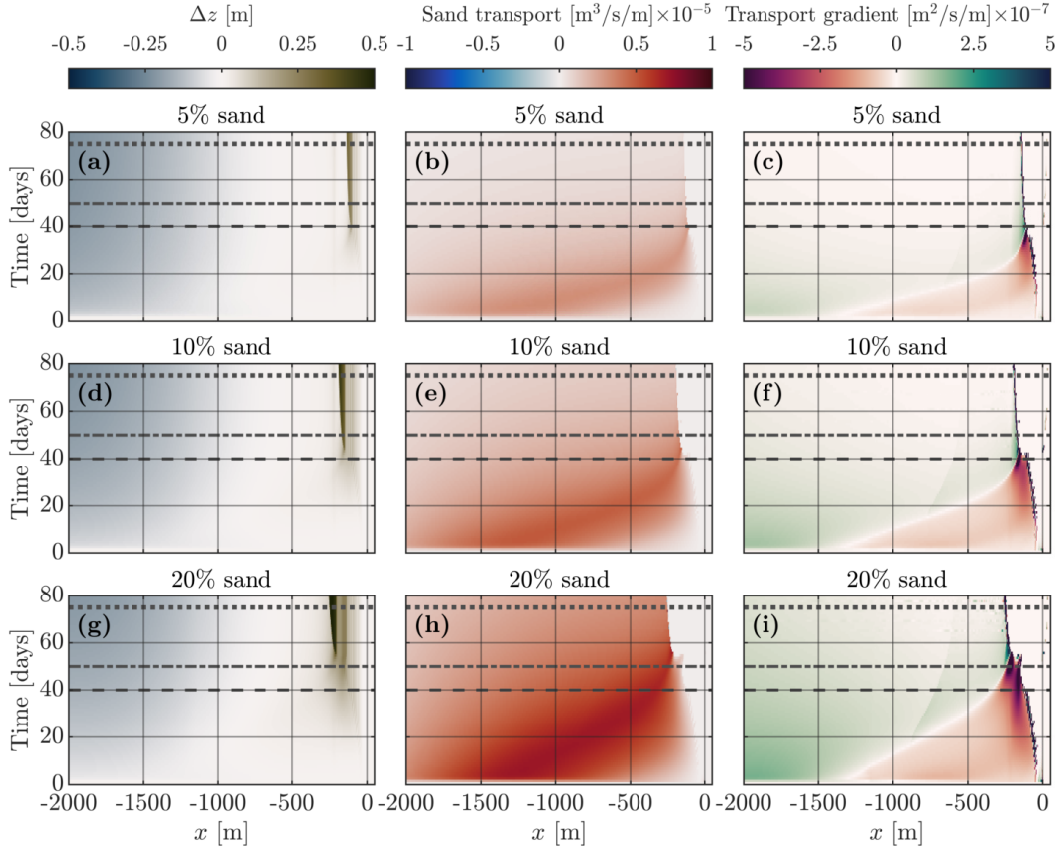


Figure 5. Bed level change (left column), sand transport (middle column) and sand transport gradient (right column) for three different initial sand fractions: 5% (upper row), 10% (middle row) and 20% (lower row). The horizontal dashed lines correspond to the different panels in Figure 6 (dashed line: 40 days, panel 6a; dash-dotted line: 50 days, panel 6b; and dotted line: 75 days, panel 6c).

230

231

232

233

234

235

236

237

Initially, sediment transport is maximal in deeper water ($x = 1000\text{--}1500$ m with water depth $d = 2 - 3$ m at $t = 0$ in Figure 5e). Sand is eroded seaward of this sand transport peak (positive transport gradient in Figure 5f) and deposited landward (negative transport gradient). The winnowed sand body migrates landward, driven by wave asymmetry and a gradual depletion of sand in the sand-mud mixture. The moment the peak sand transport rate is close to the shore ($x = 200$ m at $t = 40$ days in Figure 5e), the decrease in transport in landward direction is concentrated over such a narrow zone that a chenier crest emerges (Figure 5d).

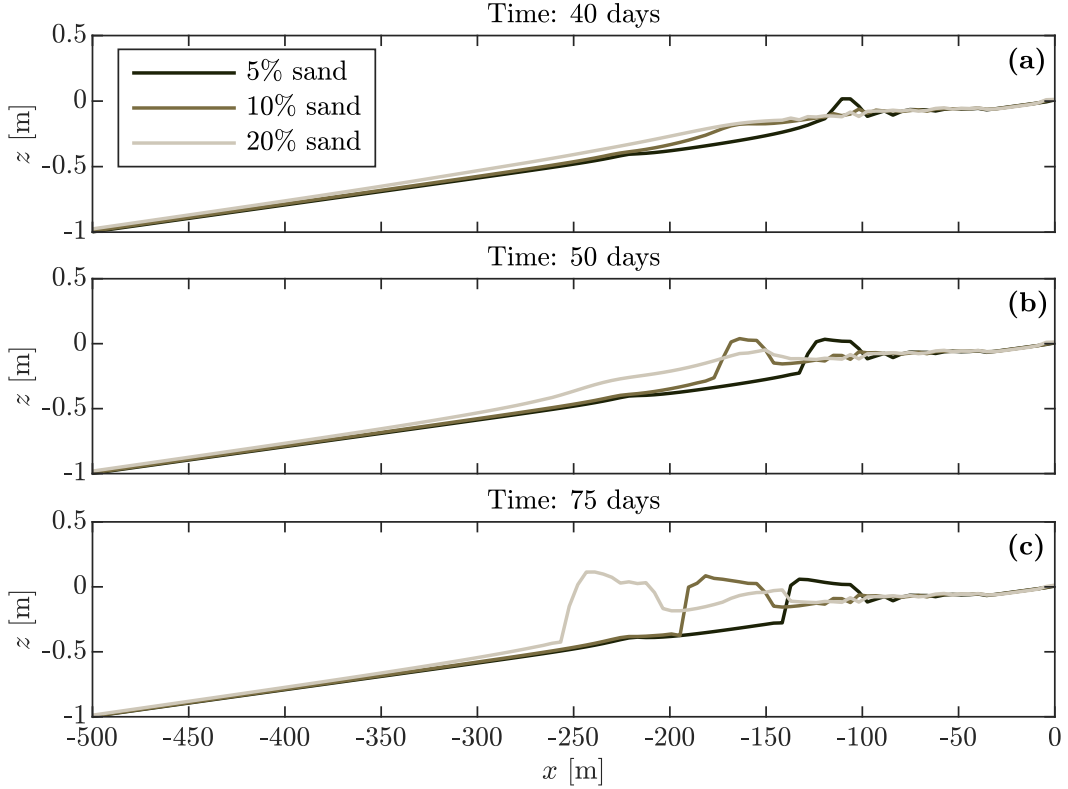


Figure 6. Bed level evolution at three moments in time (panel (a) after 40 days, panel (b) after 50 days, and panel (c) after 75 days) for three different initial sand fractions: 5% (darkest shade brown), 10% (medium shade brown) and 20% (lightest shade brown). The three sand fraction scenarios are the same as in Figure 5.

238

3.4 Effect of the Initial Sand Fraction

239

240

241

242

243

244

245

246

247

248

249

The size of the developed cheniers, but also the time required to develop a chenier, depends not only on the waves (as evaluated above) but also on the sand fraction in the sand-mud mixture. Figure 6 shows the chenier formation process for three different initial sand fractions (different shades of brown) at three points in time (panels a-c, corresponding to the time markers in Figure 5).

Interestingly, the lowest initial sand fraction (darkest line in Figure 6) leads to the fastest emerging chenier. This initially counter-intuitive observation can be explained by sand winnowing. Because of the lower sand content in the bed, the upper bed layers are more quickly depleted of sand, the maximum transport peak converges more rapidly with the shoreline, and as a result crest formation (phase 3) starts earlier. The onset of crest formation for the scenario with 10% sand is visible around $x = -170$ m (Figure

250 6a) and for the scenario with 20% sand around $x = -230$ m (Figure 6b). The chenier
 251 crest is located where the fine sand layer (which slowly built out from the water line) con-
 252 verges with the steepest transport gradients (see Figures 5c, 5f and 5i).

253 3.5 Effect of Tides

254 The model scenarios evaluated up to now assume a constant water level. In the fol-
 255 lowing scenarios a single tidal component (K1, the dominant constituent) is prescribed
 256 as boundary condition with an amplitude of 0.5 m (the amplitude of spring tide in De-
 257 mak). Chenier formation under average storm conditions and the simplified tide is vi-
 sualized in Figure 7.

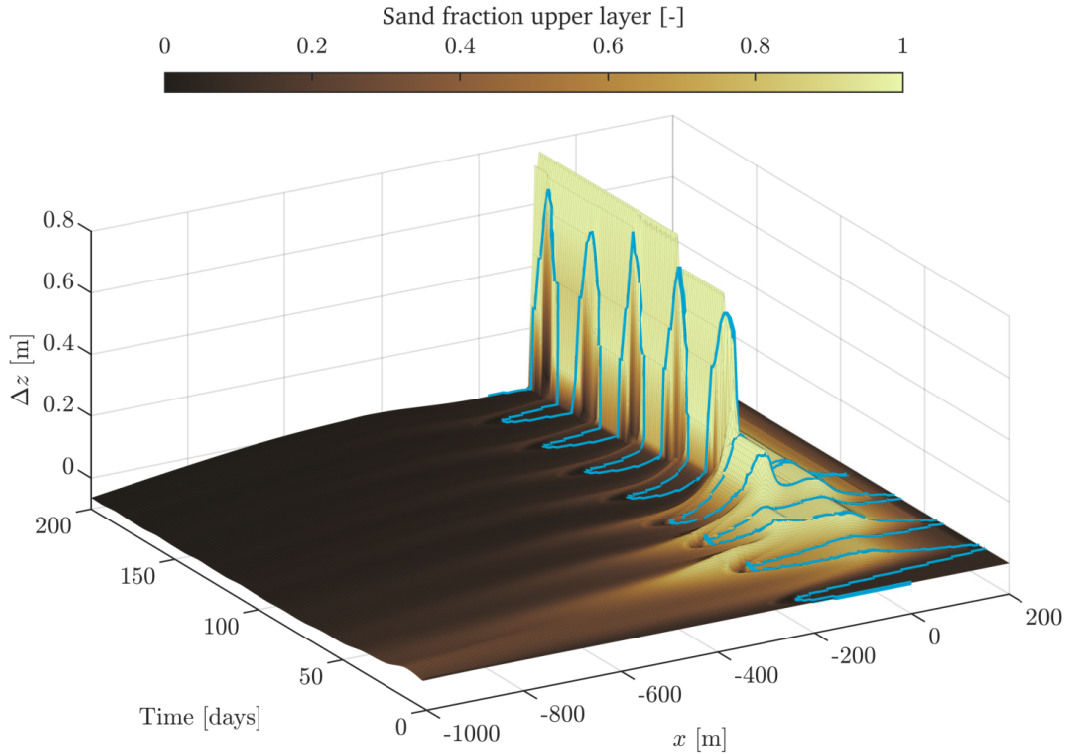


Figure 7. Changes in bed elevation and composition over time. The horizontal axes represent the time and x-coordinate, and the vertical axis the elevation change relative to the initial profile. The colors show the sand fraction of the upper bed layer. At the offshore boundary, a constant wave condition is applied (average storm; $H_s = 1.3$ m and $T_p = 5.6$ s), a simple tidal signal ($a_{K1} = 0.5$ m) and starting from a fully mixed bed with a sand content of 10%. The blue line shows the water line at each time step.

259 The effect of tides on chenier formation can be inferred from Figure 7 (with tides)
260 and Figure 1 (same wave conditions, but constant water level). With tidal forcing, the
261 chenier develops more slowly compared to a simulation without tides (crest formation
262 after 90 days versus 43 days), and the crest is located more landward (around $x = -70$
263 m versus $x = -155$ m) and higher (around $z = 0.55$ m above MSL versus $z = 0.10$ m
264 above MSL).

265 This difference is related to the time and spatially varying water depths and bed
266 shear stresses. In the intertidal zone, sand is only transported when the bed is submerged
267 (the migrating water line is indicated with the blue line in Figure 7), and therefore the
268 chenier cannot develop during periods of emergence. This explains the slower develop-
269 ment of the chenier under tidal conditions. The height of the chenier crest is limited by
270 two factors: the water surface and the available volume of sand. The maximum water
271 surface is higher for tidal conditions, leading to a higher crest height. But in addition
272 to this, the waves propagate further landward during high tide, thus enlarging the bed
273 surface from which sand can be winnowed (i.e.: more sand is available under tidal con-
274 ditions, favouring a higher chenier).

275 3.6 Realistic Boundary Conditions

276 As a final step, chenier formation under realistic time series for the wave conditions
277 and water levels is evaluated. Wave conditions were derived from the Wave Watch III
278 hindcast data (The WAVEWATCH III Development Group, 2019) for the NW monsoon
279 season between 1 December 2016 and 1 March 2017. The water levels were calculated
280 using all tidal constituents derived from the water level data measured at Semarang (Tas
281 et al., 2020). A morphological factor of 5 was applied to realise bed level changes within
282 acceptable computational periods (Figure 8).

283 During the first weeks, the wave height is low (rarely exceeding 0.8 m). As a re-
284 sult, sand is only winnowed from a narrow nearshore zone and transported to the coast-
285 line (phase 1 and 2), but the amount of sand is insufficient to develop into a crest (phase
286 3). A fine sand layer develops relatively high in the profile, above MSL.

287 Winnowing and sand transport occur over a much wider zone during the first storm
288 ($t = 100$ days), and more sand is transported landward. This leads to sufficient nearshore
289 sand availability for the formation of a chenier crest. The crest is formed at the seaward
290 edge of the sand layer, which is relatively far landward.

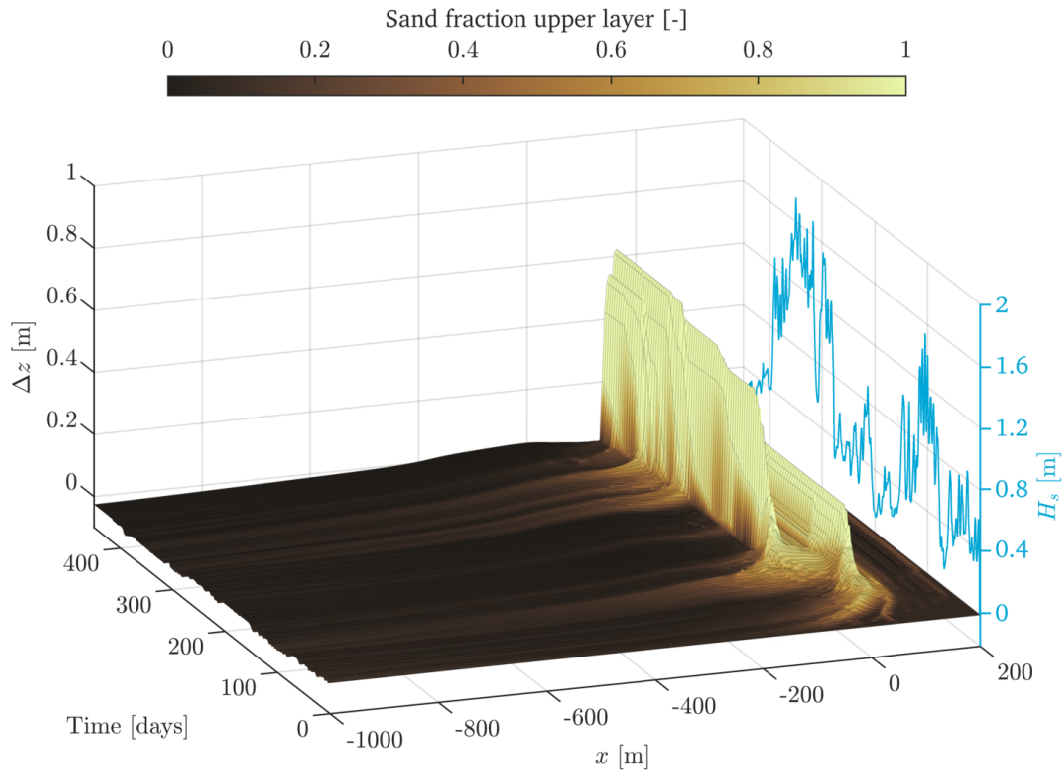


Figure 8. Changes in bed elevation and composition over time. The horizontal axes represent the time and x-coordinate, and the vertical axis the elevation change relative to the initial profile. On a secondary z-axis (blue axis) the significant wave height at the offshore boundary is given. The colors show the sand fraction of the upper bed layer. At the offshore boundary, a time series for the wave conditions and water levels representative for the NW monsoon season were applied.

291 After a brief period with calmer conditions (during which the chenier remains static
 292 although sand is transported landward to form a fine sand sheet seaward of the chenier),
 293 a new storm initiates a second phase of substantial onshore sand transport and the for-
 294 mation of a second chenier crest. This crest is again located at the seaward edge of the
 295 sand layer, and is thus located more seaward than the first chenier crest. This crest quickly
 296 grows in height and shelters the older chenier crest from wave action, until it stabilises
 297 with its crest around the highest tidal levels. Later storm periods transport new volumes
 298 of sand nearshore, leading to a slight widening of the chenier crest in the seaward direc-
 299 tion.

300 A notable difference between this model scenario with varying boundary conditions
 301 and the previous scenarios with constant boundary conditions, is the role of the calmer

302 periods between storms. The wave energy during these calm periods is too weak to trans-
 303 port sufficient sand nearshore to develop into a chenier crest. However, there is still on-
 304 shore sand transport. This sand supplied during calm conditions provides the material
 305 for rapid chenier formation during stormy periods. Therefore cheniers may more rapidly
 306 emerge during storms following a period of relatively calm conditions.

307 4 Discussion

308 We have numerically investigated chenier formation for a range of hydrodynamic
 309 boundary conditions representing the environmental conditions near Demak, Indonesia
 310 (see Table 1). A chenier developed for 18 of the 27 scenarios: the only conditions for which
 311 no chenier crest developed were for smaller, sea breeze-induced waves. These various hy-
 312 drodynamic conditions influence the location where the chenier emerges (x_{crest}) and the
 313 time it takes for the chenier to develop (t_{crest}). Figure 9 summarises x_{crest} and t_{crest} for
 314 all scenarios with chenier development. Here, the moment of crest formation was defined
 315 as the moment the chenier crest reaches 50% of its final crest height, which coincides with
 316 the moment of rapid crest heightening (when the highest transport gradients reach the
 317 shoreline - see also Figure 5).

318 The chenier crest develops further offshore for scenarios with higher waves (filled
 319 markers) and/or higher initial sand content (yellow markers). Both contribute to a larger
 320 sand volume in the nearshore, which allows the initial nearshore sand layer to build out
 321 further offshore. A larger tidal range slows down the speed of chenier formation (high
 322 t_{crest}), as the varying water levels lead to a larger range in water depths and bed shear
 323 stresses. The diagram also provides more details on the role of the initial sediment sub-
 324 strate. The results in section 3.4) suggested that a chenier develops slower for higher sand
 325 content but closer inspection of Figure 9 reveals that this is only true for high wave
 326 conditions or in the absence of tide. For moderate wave ($H_s = 1.3$ m) and tide ($a_{K1} =$
 327 0.25–0.5 m) conditions (open triangles and squares) the duration of crest formation is
 328 independent of the initial sand content.

329 Chenier formation has always been associated with extreme storms (e.g. Woodroffe
 330 and Grime (1999); Dougherty and Dickson (2012)), but our model results suggest that
 331 also milder storm conditions are important for chenier formation. This can be explained
 332 with the three phases which drive the formation of cheniers: winnowing, onshore trans-
 333 port, and crest formation. Milder storms regularly occurring during the NW monsoon

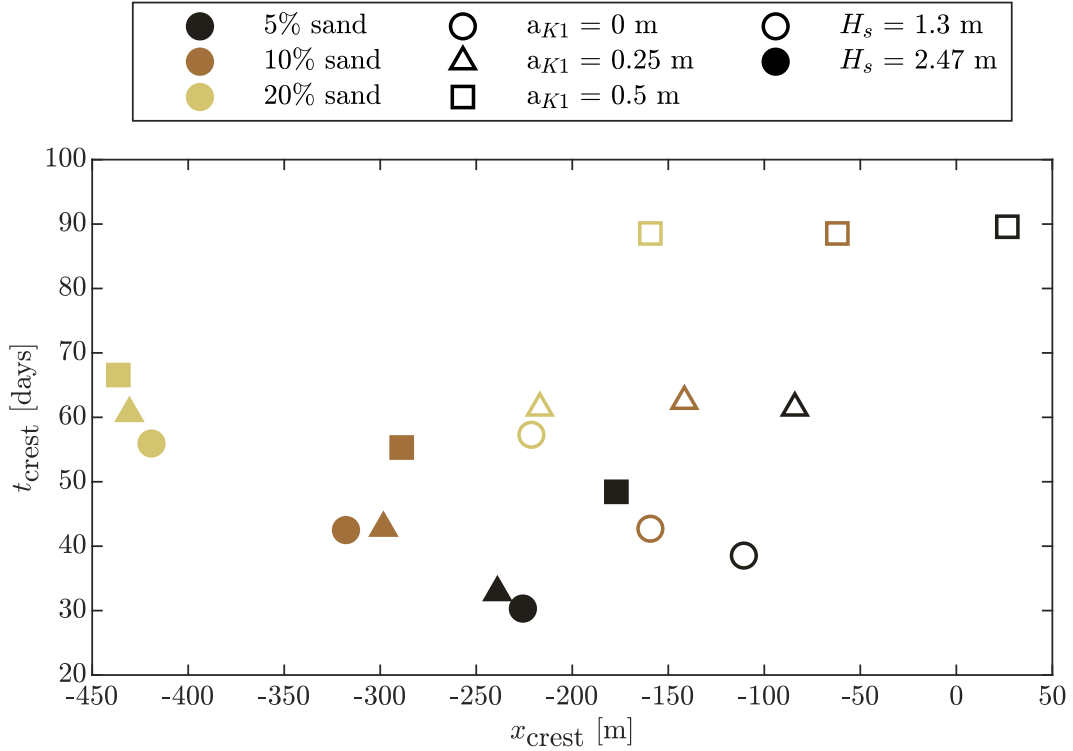


Figure 9. Location of the chenier crest (horizontal axis) and duration until crest development (vertical axis) for all scenarios that resulted in a chenier (18 out of 27 scenarios described in Table 1, excluding the sea breeze wave conditions). The shape of the data points relate to the tidal range (circle: no tide, triangle: neap tide, square: spring tide), the colours represent the sand content of the bed (lighter for higher sand content) and the two wave conditions are distinguished by the fill (no fill: average storm conditions, filled: extreme storm conditions).

334 season are already energetic enough to activate all three phases of chenier formation. Fur-
 335 thermore, small amounts of sand are still transported nearshore during calmer periods
 336 in-between. While the winnowing phase has been described qualitatively in previous work
 337 (Augustinus, 1980; Rhodes, 1982; Woodroffe & Grime, 1999; Nardin & Fagherazzi, 2018;
 338 Anthony et al., 2019), our findings provide the first quantitative investigation on this win-
 339 nowing process in relation to the development of individual cheniers.

340 Our model results further suggest that the largest timescales are associated with
 341 phase 1 (winnowing) and 2 (onshore transport). The actual crest formation, however,
 342 is very fast (see also Section 3.3). In our model approach the timescales of winnowing
 343 are dependent on the state of the initial sediment bed (fully mixed), and therefore it takes
 344 a long time for the chenier to develop. It is also not realistic that storm conditions oc-

345 cur uninterrupted for 50 days (as in our moderate and high storm conditions simulations).
346 However, a sequence of storms (and calmer periods and seasons in between) may even-
347 tually set up a sufficiently pre-sorted situation, which could allow a regular, short storm
348 to form a chenier.

349 The scenario with a realistic time series for the wave conditions and water levels
350 reveal the development of a second chenier crest, seaward of the first crest. This may seem
351 similar to bar systems which often have multiple shore-parallel bars occurring simulta-
352 neously (Short, 1991; Ruessink et al., 2003; Walstra et al., 2012). However, in contrast
353 to submerged bars, chenier crests quickly develop to a height around or above MSL, thus
354 emerging during (part of) each tidal cycle. As a result, the most seaward chenier crest
355 cuts off the more landward crest from tidal and wave influences, blocking any further sand
356 supply and effectively stopping its dynamics. This is in agreement with observations by
357 Woodroffe et al. (1983) on the chenier plain in the Firth of Thames, New Zealand.

358 By using the stratigraphy schematisation in Delft3D to model separate bed lay-
359 ers, we modelled the winnowing process in detail. We showed that even for very low sand
360 content (5%), a chenier can be formed. This agrees with the findings of Nardin and Fagher-
361 azzi (2018) that sand availability usually is not the limiting factor in chenier formation
362 (except for extremely low sand contents). This finding explains the presence of cheniers
363 in areas without a nearby source of coarser sediments, e.g. in Demak, Indonesia.

364 Possibly the largest limitation of our modelling approach is the absence of sand-
365 mud interactions. In our model set-up, a cohesive (mud) and a non-cohesive (sand) frac-
366 tion were considered independently: the sand fraction is mainly transported as suspended
367 load due to wave asymmetry once a critical bed shear stress based on the Shields curve
368 is exceeded; the mud fraction is transported as a suspended load, once the critical bed
369 shear stress for erosion is exceeded. However, a sand-mud mixture will behave as a co-
370 hesive mixture when the mud content is higher than 30% (van Ledden et al., 2004). Such
371 a mixture will typically have a higher critical bed shear stress for erosion (van Rijn, 2020).
372 Furthermore, we assumed a relatively low settling velocity and critical bed shear stress
373 for the mud fraction. Altogether, this means that our model results may overestimate
374 the speed (and extent) at which winnowing takes place.

5 Conclusions

A numerical model (Delft3D) is used to analyse how cheniers develop through wave-induced winnowing and transport. We identify three phases in chenier genesis: (1) winnowing, when the mud is washed out and the upper layer of the sediment becomes increasingly sandy; (2) sand transport, when the sand in the upper layer is transported landward; and (3) crest formation, when the sand culminates at one point, resulting in a rapid heightening of the chenier crest. Winnowing takes place when mud is eroded from the bed and brought into suspension (when $\tau_{cw,max} > \tau_{cr,e}$), leaving behind a fine layer of sand. Sand transport takes place when the threshold for the initiation of motion is exceeded (when $v_{eff} > v_{cr}$). The onshore sand transport is mainly driven by wave asymmetry, and is supply-limited (directly depending on the winnowing). Crest formation occurs when the peak of the sand transport rate converges at the shoreline, locally generating steep negative transport gradients resulting in rapid sedimentation.

The model study suggests that chenier formation does not require extreme storm conditions. Winnowing and onshore sand transport (phases 1 and 2) already take place under calm conditions, but crest formation (phase 3) requires sufficient sand to be transported nearshore. Under sea breeze conditions, the area where sand transport takes place is too small to supply sufficient sand to develop into a crest, only creating a thin nearshore layer of sand. However, average storm conditions which are exceeded several times per year, do generate sand transport over a sufficiently large spatial scale for a chenier to develop. Calm conditions therefore do not directly lead to chenier development but do result in landward transport of sand (as long as the upper layer of the bed is not depleted) which speeds up the formation of a crest during more energetic periods following that period of calm conditions.

Starting from a well-mixed bed, chenier formation is a slow process (requiring at least 8-10 weeks of uninterrupted storm conditions). Especially the time period associated with winnowing and sand transport (phases 1 and 2) is long, followed by a rapid crest formation (phase 3). The model study reveals that cheniers generally develop quicker for a lower sand content in the bed because the upper bed layers are more quickly depleted of sand. Therefore the maximum sand transport converges more rapidly with the shoreline (onset of crest formation, phase 3). On the other hand, larger tidal amplitudes slow down chenier formation, due to temporal and spatial variability of bed shear stresses and periods of emergence in the region of chenier development.

Appendix A Sediment Transport Formulae in Delft3D

A1 Bed Load Transport

The bed load transport is calculated using the empirical formula of van Rijn (1993):

$$S_b = \begin{cases} 0.006\rho_s w_s D_{50} M^{0.5} M_e^{0.7} & \text{if } v_{\text{eff}} \geq v_{\text{cr}} \\ 0 & \text{if } v_{\text{eff}} < v_{\text{cr}} \end{cases}, \quad (\text{A1})$$

where S_b is the bed load transport (in kg/m/s), ρ_s is the sediment density (in kg/m³), w_s is the settling velocity for the D_{50} of the sediment (in m/s), and D_{50} is the median diameter of the sediment fraction (in m). M is the sediment mobility number due to waves and currents (see Equation A2) and M_e is the excess sediment mobility number (see Equation A3).

The sediment mobility number, M , is defined as:

$$M = \frac{v_{\text{eff}}^2}{(s-1)gD_{50}}, \quad (\text{A2})$$

and the excess sediment mobility number, M_e , is defined as:

$$M_e = \frac{(v_{\text{eff}} - v_{\text{cr}})^2}{(s-1)gD_{50}}, \quad (\text{A3})$$

where v_{eff} is the effective velocity due to waves and currents (see Equation A4, in m/s), v_{cr} is the critical velocity for the initiation of motion (see Equation A6, in m/s), s is the relative density (see Equation A5) and g is the gravitational acceleration (in m/s²).

The effective velocity due to waves and currents, v_{eff} , is:

$$v_{\text{eff}} = \sqrt{v_{\text{R}}^2 + U_{\text{on}}^2}, \quad (\text{A4})$$

where v_{R} is the magnitude of the depth-averaged current velocity (in m/s) and U_{on} is the onshore-directed, high frequency near-bed orbital velocity (in m/s), calculated using a modification of the method of Isobe and Horikawa (1982) by Grasmeijer and van Rijn (1998).

The relative density s is defined as:

$$s = \frac{\rho_s}{\rho_w}. \quad (\text{A5})$$

The critical velocity for the initiation of motion is determined based on a parametrization of the Shields curve (van Rijn, 1993; Soulsby, 1997):

$$v_{\text{cr}} = \begin{cases} 0.19D_{50}^{0.1} \log_{10} \left(\frac{4h}{D_{90}} \right) & \text{if } D_{50} \leq 0.5 \text{ mm} \\ 8.5D_{50}^{0.6} \log_{10} \left(\frac{4h}{D_{90}} \right) & \text{if } 0.5 \text{ mm} < D_{50} \leq 2 \text{ mm} \end{cases}, \quad (\text{A6})$$

435 where h is the water depth (in m) and D_{90} is the sediment diameter (in m) for which
 436 90% of the sediment has a smaller diameter, and is based on the composition of the lo-
 437 cal sediment mixture. In this case, $D_{90} = 1.5D_{50}$.

438 The bed load transport S_b consists of a current-driven component, $S_{b,c}$, and a wave-
 439 driven component, $S_{b,w}$:

$$440 \quad S_b = \sqrt{S_{b,c}^2 + S_{b,w}^2 + 2|S_{b,c}||S_{b,w}|\cos(\varphi)}, \quad (\text{A7})$$

441 with φ the angle between the current and wave direction. From this equation it follows
 442 that the current-driven and wave-driven components, $S_{b,c}$ and $S_{b,w}$ respectively, can be
 443 calculated as:

$$444 \quad S_{b,c} = \begin{cases} \frac{S_b}{\sqrt{1+r^2+2|r|\cos(\varphi)}} & \text{if } r \leq 100 \\ 0 & \text{if } r > 100 \end{cases}, \quad (\text{A8})$$

$$445 \quad |S_{b,w}| = \begin{cases} r|S_{b,c}| & \text{if } r \geq 0.01 \\ 0 & \text{if } r < 0.01 \end{cases}, \quad (\text{A9})$$

447 with:

$$448 \quad r = \left(\frac{|U_{\text{on}}| - v_{\text{cr}}}{|v_{\text{R}}| - v_{\text{cr}}} \right)^3. \quad (\text{A10})$$

449 **A2 Suspended Transport**

450 Suspended transport is described by an advection-diffusion equation. In depth-averaged
 451 mode ($\partial/\partial z = 0$) and assuming longshore uniformity ($\partial/\partial y = 0$) this equation reads:

$$452 \quad \frac{\partial ch}{\partial t} + \frac{\partial Uch}{\partial x} - h \frac{\partial}{\partial x} \left(\epsilon_{s,x} \frac{\partial c}{\partial x} \right) = E - D \quad (\text{A11})$$

453 where c is the concentration (in kg/m^3), h is the water depth (in m), U is the depth-averaged
 454 velocity in x-direction (in m/s), w_s is the settling velocity (in m/s), $\epsilon_{s,x}$ is the horizon-
 455 tal eddy diffusivity (in m^2/s), E is the erosion flux (in $\text{kg}/\text{m}^2/\text{s}$) and D is the deposi-
 456 tion flux (in $\text{kg}/\text{m}^2/\text{s}$). In Equation A11, the second term gives the advective transport,
 457 the third term the diffusive transport and the right hand side represents the source and
 458 sink terms (to and from the bed). For cohesive sediment, the erosion and depositional
 459 fluxes are calculated with the Partheniades erosion formulation (Partheniades, 1965) and
 460 a permanent deposition flux (Winterwerp, 2007):

$$461 \quad E = M_{\text{ero}} S(\tau_{\text{cw,max}}, \tau_{\text{cr,e}}), \quad (\text{A12})$$

462 and

$$463 \quad D = w_s c_b, \quad (\text{A13})$$

464 where M_{ero} is an erosion parameter (in $\text{kg}/\text{m}^2/\text{s}$), $S(\tau_{\text{cw,max}}, \tau_{\text{cr,e}})$ is an erosion function
 465 (see Equation A14) and c_b is the average sediment concentration near the bed (in kg/m^3).

466 The erosion function is defined as:

$$467 \quad S(\tau_{\text{cw,max}}, \tau_{\text{cr,e}}) = \begin{cases} \left(\frac{\tau_{\text{cw,max}}}{\tau_{\text{cr,e}}} - 1 \right) & \text{if } \tau_{\text{cw,max}} > \tau_{\text{cr,e}} \\ 0 & \text{if } \tau_{\text{cw,max}} \leq \tau_{\text{cr,e}} \end{cases}, \quad (\text{A14})$$

468 Here, $\tau_{\text{cr,e}}$ is the critical bed shear stress for erosion (in N/m^2) and $\tau_{\text{cw,max}}$ is the max-
 469 imum bed shear stress due to current and waves (in N/m^2). This maximum bed shear
 470 stress is computed with the parametrisation of Soulsby et al. (1993):

$$471 \quad |\tau_{\text{cw,max}}| = Z(|\tau_c| + |\tau_w|), \quad (\text{A15})$$

472 where τ_c is the bed shear stress due to currents (in N/m^2), τ_w is the bed shear stress due
 473 to waves (in N/m^2), and Z is a dimensionless parameter.

474 The bed shear stress due to currents, τ_c , is defined as

$$475 \quad \tau_c = \frac{g\rho_w U|U|}{C^2}, \quad (\text{A16})$$

476 where U is the depth-averaged velocity (in m/s) and C is the Chézy coefficient (in $\text{m}^{1/2}/\text{s}$).

477 The magnitude of the bed shear stress due to waves alone is defined as:

$$478 \quad \tau_w = 0.5\rho_w f_w u_{\text{orb}}^2, \quad (\text{A17})$$

479 where f_w is the wave friction factor (defined in Equation A19) and u_{orb} is the peak or-
 480 bital velocity (in m/s) and can be calculated using linear wave theory:

$$481 \quad u_{\text{orb}} = \frac{\sqrt{\pi}}{4} \frac{H_{\text{rms}}\omega}{\sinh(kh)}. \quad (\text{A18})$$

482 Here H_{rms} is the root-mean-square wave height (in m), $\omega = 2\pi/T$ is the wave angu-
 483 lar frequency (in s^{-1}) and $k = 2\pi/L$ is the wave number (in m^{-1}) which can be derived
 484 from the linear wave dispersion relationship.

485 The wave friction factor under pure oscillatory flow is calculated following Swart
 486 (1974):

$$487 \quad f_w = \begin{cases} 0.00251 \exp \left[5.21 \left(\frac{A}{k_s} \right)^{-0.19} \right] & \text{if } \frac{A}{k_s} > \frac{\pi}{2} \\ 0.3 & \text{if } \frac{A}{k_s} \leq \frac{\pi}{2} \end{cases}, \quad (\text{A19})$$

488 where k_s is the Nikuradse roughness height (in m) (which can be derived from the Chézy
 489 coefficient, see Equation A21) and A , the orbital excursion length, equals:

$$490 \quad A = \frac{u_{\text{orb}}}{\omega}. \quad (\text{A20})$$

491 The Nikuradse roughness height is derived from the Chézy coefficient using the formu-
 492 lation of White-Colebrook:

$$493 \quad k_s = 12h10^{-C/18} \quad (\text{A21})$$

494 The dimensionless parameter Z from Equation A15 is defined as:

$$495 \quad Z = 1 + aX^m(1 - X)^n, \quad (\text{A22})$$

496 with:

$$497 \quad X = \frac{|\tau_c|}{|\tau_c| + |\tau_w|}. \quad (\text{A23})$$

498 The value of the parameters a , m and n can be determined through the following ex-
 499 pression:

$$500 \quad \chi = (\chi_1 + \chi_2|\cos \varphi|^J) + (\chi_3 + \chi_4|\cos \varphi|^J) \log_{10} \left(\frac{f_w}{C} \right) \quad (\text{A24})$$

501 where φ is the angle between the current direction and the direction of wave propaga-
 502 tion and χ represents a , m or n . The fitting coefficients based on Fredsøe (1984) are used,
 see Table A1.

Table A1. Fitting coefficients for wave-current boundary layer model, using FR84 (Fredsøe, 1984)

FR84	χ_1	χ_2	χ_3	χ_4
a	-0.06	1.70	-0.29	0.29
m	0.67	-0.29	0.09	0.42
n	0.75	-0.27	0.11	-0.02
J	0.80			

503
 504 In addition to the suspended transport via advection and diffusion (which in this
 505 case is mostly mud transport), there is also suspended sand transport due to wave asym-
 506 metry. This component represents the effect of asymmetric wave orbital velocities on sus-
 507 pended sediment transport within about 0.5 m of the bed and can be approximated fol-
 508 lowing van Rijn et al. (2001):

$$509 \quad S_{s,w} = f_{\text{SUSW}}\gamma U_A S_S, \quad (\text{A25})$$

510 where f_{SUSW} is a user-defined tuning parameter, γ is the phase lag coefficient ($\gamma = 0.2$),
 511 U_A is the velocity asymmetry value (in m/s, see Equation A26) and S_S is the suspended
 512 sediment load (in kg/m/s, see Equation A27).

513 The velocity asymmetry value, U_A , is defined as:

$$514 \quad U_A = \frac{U_{\text{on}}^4 - U_{\text{off}}^4}{U_{\text{on}}^3 + U_{\text{off}}^3}, \quad (\text{A26})$$

515 and the suspended sediment load, S_S , as:

$$516 \quad S_S = 0.007\rho_s D_{50} M_e. \quad (\text{A27})$$

517 In Delft3D, this transport component is included in the bed load vector, because it does
518 not exhibit the relaxation effects of an advection-diffusion relation (Deltares, 2021).

519 **Acknowledgments**

520 This work is part of the BioManCO project with project number 14753, which is (partly)
521 financed by NWO Domain Applied and Engineering Sciences, and co-financed by Boskalis
522 Dredging and Marine Experts, Van Oord Dredging and Marine Contractors bv, Deltares,
523 Witteveen+Bos and Wetlands International. The BioManCO project is a collaboration
524 between TU Delft, NIOZ and UNDIP and makes use of the framework set up by Build-
525 ing with Nature Indonesia, a programme by Ecoshape, Wetlands International, the In-
526 donesian Ministry of Marine Affairs and Fisheries (MMAF), the Indonesian Ministry of
527 Public Works and Housing (PU) and other partners.

528 **References**

- 529 Alferink, M. (2022). *Wave transmission through permeable structures in Demak In-*
530 *donesia* (MSc thesis, Delft University of Technology). Retrieved from [http://](http://resolver.tudelft.nl/uuid:23dc0cc4-9658-44ab-a067-5800a0731853)
531 resolver.tudelft.nl/uuid:23dc0cc4-9658-44ab-a067-5800a0731853
- 532 Anthony, E. J., Brunier, G., Gardel, A., & Hiwat, M. (2019). Chenier Morphody-
533 namics on the Amazon-Influenced Coast of Suriname, South America: Impli-
534 cations for Beach Ecosystem Services. *Frontiers in Earth Science*, 7(March),
535 1–20. doi: 10.3389/feart.2019.00035
- 536 Anthony, E. J., Gardel, A., Gratiot, N., Proisy, C., Allison, M. A., Dolique, F., &
537 Fromard, F. (2010). The Amazon-influenced muddy coast of South America:
538 A review of mud-bank-shoreline interactions. *Earth-Science Reviews*, 103,
539 99–121. doi: 10.1016/j.earscirev.2010.09.008
- 540 Augustinus, P. G. E. F. (1980). Actual development of the chenier coast of Suri-
541 name (South America). *Sedimentary Geology*, 26(1-3), 91–113. doi: 10.1016/
542 0037-0738(80)90007-X

- 543 Augustinus, P. G. E. F. (1989). Cheniers and chenier plains: A general introduction.
544 *Marine Geology*, *90*(4), 219–229. doi: 10.1016/0025-3227(89)90126-6
- 545 Belperio, A. P., Gostin, V. A., Cann, J. H., & Murray-Wallace, C. V. (1988).
546 Sediment-organism zonation and the evolution of Holocene tidal sequences in
547 Southern Australia. In P. L. de Boer, A. van Gelder, & S. D. Nio (Eds.), *Tide-*
548 *influenced sedimentary environments and facies* (pp. 475–497). Dordrecht, the
549 Netherlands: D. Reidel Publishing Company.
- 550 Booij, N., Ris, R. C., & Holthuijsen, L. H. (1999). A third-generation wave model
551 for coastal regions: 1. Model description and validation. *Journal of Geophysical*
552 *Research*, *104*(C4), 7649–7666. doi: 10.1029/98JC02622
- 553 Deltares. (2021). *Delft3D-FLOW. Simulation of multi-dimensional hydrodynamic*
554 *flows and transport phenomena, including sediments. User Manual* (Tech.
555 Rep.). Delft: Author. Retrieved from [https://content.oss.deltares.nl/](https://content.oss.deltares.nl/delft3d/manuals/Delft3D-FLOW_User_Manual.pdf)
556 [delft3d/manuals/Delft3D-FLOW_User_Manual.pdf](https://content.oss.deltares.nl/delft3d/manuals/Delft3D-FLOW_User_Manual.pdf)
- 557 Deltares, & BioManCO. (2019). *Sediment analysis of Demak* (Tech. Rep.). Delft:
558 Deltares.
- 559 Dougherty, A. J., & Dickson, M. E. (2012). Sea level and storm control on the evo-
560 lution of a chenier plain, Firth of Thames, New Zealand. *Marine Geology*, *307-*
561 *310*, 58–72. doi: 10.1016/j.margeo.2012.03.003
- 562 Fredsøe, J. (1984). Turbulent boundary layer in wave-current motion. *Journal of Hy-*
563 *draulic Engineering*, *110*(8), 1103–1120. doi: [https://doi.org/10.1061/\(ASCE\)](https://doi.org/10.1061/(ASCE)0733-9429(1984)110:8(1103))
564 [0733-9429\(1984\)110:8\(1103\)](https://doi.org/10.1061/(ASCE)0733-9429(1984)110:8(1103))
- 565 Grasmeyer, B. T., & van Rijn, L. C. (1998). Breaker Bar Formation and Migra-
566 tion. In *26th international conference on coastal engineering* (pp. 2750–2758).
567 doi: 10.1061/9780784404119.208
- 568 Isobe, M., & Horikawa, K. (1982). Study on water particle velocities of shoaling and
569 breaking waves. *Coastal Engineering in Japan*, *23*, 109–123. doi: 10.1080/
570 [05785634.1982.11924340](https://doi.org/10.1080/05785634.1982.11924340)
- 571 Lesser, G. R., Roelvink, J. A., van Kester, J. A. T. M., & Stelling, G. S. (2004). De-
572 velopment and validation of a three-dimensional morphological model. *Coastal*
573 *Engineering*, *51*(8-9), 883–915. doi: 10.1016/j.coastaleng.2004.07.014
- 574 Manning, A. J., & Dyer, K. R. (2007). Mass settling flux of fine sediments in North-
575 ern European estuaries: Measurements and predictions. *Marine Geology*,

- 576 245(1-4), 107–122. doi: 10.1016/j.margeo.2007.07.005
- 577 Nairn, R. B., Roelvink, J. A., & Southgate, H. N. (1991). Transition Zone Width
578 and Implications for Modelling Surfzone Hydrodynamics. In B. L. Edge (Ed.),
579 *22nd international conference on coastal engineering 1990* (pp. 68–81). American
580 Society of Civil Engineers. doi: 10.1061/9780872627765.007
- 581 Nardin, W., & Fagherazzi, S. (2018). The Role of Waves, Shelf Slope, and Sediment
582 Characteristics on the Development of Erosional Chenier Plains. *Geophysical
583 Research Letters*, 45(16), 8435–8444. doi: 10.1029/2018GL078694
- 584 Otvos, E. G., & Price, W. A. (1979). Problems of chenier genesis and terminology -
585 An overview. *Marine Geology*, 31(3-4), 251–263. doi: 10.1016/0025-3227(79)
586 90036-7
- 587 Partheniades, E. (1965). Erosion and deposition of cohesive soils. *Journal of
588 the Hydraulics Division*, 91(1), 105–139. doi: [https://doi.org/10.1061/
589 JYCEAJ.0001165](https://doi.org/10.1061/JYCEAJ.0001165)
- 590 Prost, M. T. (1989). Coastal dynamics and chenier sands in French Guiana. *Marine
591 Geology*, 90(4), 259–267. doi: 10.1016/0025-3227(89)90128-X
- 592 Pujos, M., Pons, J.-C., & Parra, M. (2001). Les minéraux lourds des sables du
593 littoral de la Guyane française: bilan sur l'origine des dépôts de la plate-
594 forme des Guyanes. *Oceanologica Acta*, 24(SUPPL). doi: 10.1016/
595 s0399-1784(01)00093-7
- 596 Reniers, A. J. H. M., Roelvink, J. A., & Thornton, E. B. (2004). Morphodynamic
597 modeling of an embayed beach under wave group forcing. *Journal of Geophysical
598 Research*, 109(C01030). doi: 10.1029/2002jc001586
- 599 Rhodes, E. G. (1982). Depositional model for a chenier plain, Gulf of Carpentaria,
600 Australia. *Sedimentology*, 29, 201–221. doi: 10.1111/j.1365-3091.1982.tb01719
601 .x
- 602 Rosen, T., & Xu, Y. J. (2011). Riverine sediment inflow to Louisiana Chenier Plain
603 in the Northern Gulf of Mexico. *Estuarine, Coastal and Shelf Science*, 95(2-3),
604 279–288. doi: 10.1016/j.ecss.2011.09.013
- 605 Ruessink, B. G., Wijnberg, K. M., Holman, R. A., Kuriyama, Y., & van Enkevort,
606 I. M. J. (2003). Intersite comparison of interannual nearshore bar behavior.
607 *Journal of Geophysical Research*, 108(C8). doi: 10.1029/2002JC001505
- 608 Short, A. D. (1991). Macro-Meso Tidal Beach Morphodynamics - An Overview.

- 609 *Journal of Coastal Research*, 7(2), 417–436. Retrieved from [https://](https://www.jstor.org/stable/4297847)
610 www.jstor.org/stable/4297847
- 611 Soulsby, R. L. (1997). *Dynamics of marine sands*. London: Thomas Telford. Re-
612 trieved from <http://www.icevirtuallibrary.com/content/book/100318>
- 613 Soulsby, R. L., Hamm, L., Klopman, G., Myrhaug, D., Simons, R. R., & Thomas,
614 G. P. (1993). Wave-current interaction within and outside the bot-
615 tom boundary layer. *Coastal Engineering*, 21, 41–69. doi: 10.1016/
616 0378-3839(93)90045-A
- 617 Soulsby, R. L., Manning, A. J., Spearman, J., & Whitehouse, R. J. S. (2013). Set-
618 tling velocity and mass settling flux of flocculated estuarine sediments. *Marine*
619 *Geology*, 339, 1–12. doi: 10.1016/j.margeo.2013.04.006
- 620 Svendsen, I. A. (1984). Wave heights and set-up in a surf zone. *Coastal Engineering*,
621 8, 303–329. doi: 10.1016/0378-3839(84)90028-0
- 622 Swart, D. H. (1974). *Offshore sediment transport and equilibrium beach pro-*
623 *files* (PhD thesis, Delft University of Technology). Retrieved from [http://](http://resolver.tudelft.nl/uuid:057cb136-5f5b-484a-878d-5616fbaeda4e)
624 resolver.tudelft.nl/uuid:057cb136-5f5b-484a-878d-5616fbaeda4e
- 625 Tas, S. A. J., van Maren, D. S., Helmi, M., & Reniers, A. J. H. M. (2022). Drivers
626 of cross-shore chenier dynamics off a drowning coastal plain. *Marine Geology*,
627 445(106753). doi: 10.1016/j.margeo.2022.106753
- 628 Tas, S. A. J., van Maren, D. S., & Reniers, A. J. H. M. (2020). Observations of
629 Cross-Shore Chenier Dynamics in Demak, Indonesia. *Journal of Marine Sci-*
630 *ence and Engineering*, 8(972). doi: 10.3390/jmse8120972
- 631 The WAVEWATCH III Development Group. (2019). *User manual and system doc-*
632 *umentation of WAVEWATCH III version 6.07* (Vol. Technical Note 333; Tech.
633 Rep.). College Park, MD, USA: NOAA/NWS/NCEP/MMAB.
- 634 van Ledden, M., Van Kesteren, W. G. M., & Winterwerp, J. C. (2004). A concep-
635 tual framework for the erosion behaviour of sand-mud mixtures. *Continental*
636 *Shelf Research*, 24(1), 1–11. doi: 10.1016/j.csr.2003.09.002
- 637 van Leussen, W., & Cornelisse, J. M. (1993). The determination of the sizes and set-
638 tling velocities of estuarine flocs by an underwater video system. *Netherlands*
639 *Journal of Sea Research*, 31(3), 231–241. doi: 10.1016/0077-7579(93)90024-M
- 640 van Maren, D. S., van Kessel, T., Cronin, K., & Sittoni, L. (2015). The impact of
641 channel deepening and dredging on estuarine sediment concentration. *Conti-*

- 642 *mental Shelf Research*, 95, 1–14. doi: 10.1016/j.csr.2014.12.010
- 643 van Maren, D. S., Winterwerp, J. C., & Vroom, J. (2015). Fine sediment trans-
644 port into the hyper-turbid lower Ems River: the role of channel deepen-
645 ing and sediment-induced drag reduction. In C. K. Harris (Ed.), *12th in-*
646 *ternational conference on cohesive sediment transport*. Springer. doi:
647 10.1007/s10236-015-0821-2
- 648 van Rijn, L. C. (1993). *Principles of sediment transport in rivers, estuaries and*
649 *coastal seas*. Amsterdam, the Netherlands: Aqua Publications.
- 650 van Rijn, L. C. (2020). Erodibility of Mud–Sand Bed Mixtures. *Journal of Hydraulic*
651 *Engineering*, 146(1), 04019050. doi: 10.1061/(asce)hy.1943-7900.0001677
- 652 van Rijn, L. C., Roelvink, J. A., & ter Horst, W. (2001). *Approximation formulae*
653 *for sand transport by currents and waves and implementation in in DELFT-*
654 *MOR* (Tech. Rep.). Delft, the Netherlands: WL — Delft Hydraulics. Re-
655 trieved from [http://resolver.tudelft.nl/uuid:c226bf0a-79d6-4357-80ff-](http://resolver.tudelft.nl/uuid:c226bf0a-79d6-4357-80ff-c68c4d5f0416)
656 [-c68c4d5f0416](http://resolver.tudelft.nl/uuid:c226bf0a-79d6-4357-80ff-c68c4d5f0416)
- 657 Walstra, D. J. R., Reniers, A. J. H. M., Ranasinghe, R., Roelvink, J. A., &
658 Ruessink, B. G. (2012). On bar growth and decay during interan-
659 nual net offshore migration. *Coastal Engineering*, 60, 190–200. doi:
660 10.1016/j.coastaleng.2011.10.002
- 661 Winterwerp, J. C. (2007). On the sedimentation rate of cohesive sediment. In
662 J. P. Y. Maa, L. P. Sanford, & D. H. Schoellhamer (Eds.), *Estuarine and*
663 *coastal fine sediments dynamics: Intercoh 2003* (Vol. 8, pp. 209–226). Elsevier
664 B.V. doi: 10.1016/S1568-2692(07)80014-3
- 665 Woodroffe, C. D., Curtis, R. J., & Mclean, R. F. (1983). Development of a chenier
666 plain, Firth of Thames, New Zealand. *Marine Geology*, 53, 1–22. doi: [https://](https://doi.org/10.1016/0025-3227(83)90031-2)
667 [doi.org/10.1016/0025-3227\(83\)90031-2](https://doi.org/10.1016/0025-3227(83)90031-2)
- 668 Woodroffe, C. D., & Grime, D. (1999). Storm impact and evolution of a mangrove-
669 fringed chenier plain, Shoal Bay, Darwin, Australia. *Marine Geology*, 159,
670 303–321. doi: 10.1016/S0025-3227(99)00006-7